Inhibition of DNMT1 methyltransferase activity via glucose-regulated *O*-GlcNAcylation alters the epigenome

Heon Shin[1], Amy Leung[1], Kevin R. Costello[1,2], Parijat Senapati[1], Hiroyuki Kato[1], Michael Lee[1,2], Dimitri Lin[1], Xiaofang Tang[1], Zhen Bouman Chen[1,2], Dustin E. Schones[1,2,*]

[1]Department of Diabetes Complications and Metabolism, Beckman Research Institute, City of Hope, Duarte, CA 91010, USA; [2]Irell and Manella Graduate School of Biological Sciences, City of Hope, Duarte, CA 91010, USA

*For correspondence: dschones@coh.org

Keywords: Epigenetics / Metabolism / *O*-GlcNAcylation / Hyperglycemia

Abstract

The DNA methyltransferase activity of DNMT1 is vital for genomic maintenance of DNA methylation. We report here that DNMT1 function is regulated by *O*-GlcNAcylation, a protein modification that is sensitive to glucose levels, and that elevated *O*-GlcNAcylation of DNMT1 from high glucose environment leads to alterations to the epigenome. Using mass spectrometry and complementary alanine mutation experiments, we identified S878 as the major residue that is *O*-GlcNAcylated on DNMT1. Functional studies further revealed that *O*-GlcNAcylation of DNMT1-S878 results in an inhibition of methyltransferase activity, resulting in a general loss of DNA methylation that is preferentially at partially methylated domains (PMDs). This loss of methylation corresponds with an increase in DNA damage and apoptosis. These results establish *O*-GlcNAcylation of DNMT1 as a mechanism through which the epigenome is regulated by glucose metabolism and implicates a role for glycosylation of DNMT1 in metabolic diseases characterized by hyperglycemia.

Introduction

Protein *O*-GlcNAcylation is a dynamic and reversible post-translational modification that attaches a single *O*-linked β-*N*-acetylglucosamine to serine or threonine residues (Hart et al., 1996). It is modulated by two *O*-GlcNAc cycling enzymes, *O*-GlcNAc transferase (OGT) and *O*-GlcNAcase (OGA) that respond to metabolic signals (Hart et al., 2007; Slawson et al., 2010). Increased concentrations of UDP-GlcNAc that are observed in conditions of excess glucose lead to a general increase in protein *O*-GlcNAcylation (Walgren et al., 2003). Obesogenic diets, furthermore, have elevated protein *O*-GlcNAcylation in various human cell types, including liver cells (Guinez et al., 2011), lymphocytes (Torres and Hart, 1984), and immune cells (de Jesus et al., 2018).

As with other post-translational modifications, *O*-GlcNAcylation of proteins can influence the function and/or stability of the targeted proteins (Shin et al., 2018; Yang and Qian, 2017).

37 Thousands of proteins are targets for *O*-GlcNAcylation, including many epigenetic regulatory
38 proteins. For example, the *O*-GlcNAcylation of TET family proteins alter their activity, localization
39 and targeting (Chen et al., 2013; Ito et al., 2014; Shi et al., 2013; Zhang et al., 2014). While all
40 DNA methyltransferases have been shown to be *O*-GlcNAcylated (Boulard et al., 2020), the
41 functional consequences of this have not been previously investigated.

42 Among the DNA methyltransferase (DNMT) family of proteins, DNMT1 is imperative for
43 maintaining DNA methylation patterns during replication (Bestor and Ingram, 1983). DNMT1 is a
44 modular protein with several domains necessary for interacting with cofactors, including the BAH1
45 and BAH2 domains (Maresca et al., 2015; Ren et al., 2018). The stability and function of DNMT1
46 has been shown to be regulated through post-translational modifications, including acetylation,
47 phosphorylation, and methylation (Scott et al., 2014).

48 Partially methylated domains, large domains with a loss of DNA methylation, were
49 originally identified in cultured cell lines (Lister et al., 2009) and subsequently found to be a
50 characteristic of cancer cells (Berman et al., 2011; Brinkman et al., 2019). PMDs have also been
51 detected in non-cancerous healthy tissues, where they are associated with late replication loci
52 (Hansen et al., 2010; Zhou et al., 2018). While PMDs are generally thought to arise from a lack
53 of fidelity in maintenance methylation (Decato et al., 2020), the mechanisms responsible for the
54 establishment of PMDs have remained unclear. Here, we report that the activity of DNMT1 is
55 regulated by extracellular levels of glucose through *O*-GlcNAcylation, resulting in loss of
56 methylation within PMDs.

57

58 **Results**

59 **High glucose conditions increase *O*-GlcNAcylation of DNMT1**

60 To validate that DNMT1 can be *O*-GlcNAcylated, we treated Hep3B cells with OSMI-4 (OSMI),
61 an OGT inhibitor (Martin et al., 2018), as well as with Thiamet-G (TMG), an OGA inhibitor
62 (Elbatrawy et al., 2020). As expected, immunoblots of cellular lysate with an antibody recognizing

63 pan-*O*-GlcNAc (RL2) reveal that inhibition of OGA increased global levels of *O*-GlcNAc while
64 inhibition of OGT decreased global levels of *O*-GlcNAc (Figure 1—figure supplement 1). To
65 distinguish whether DNMT1 is *O*-GlcNAcylated, DNMT1 immunoprecipitation was performed with
66 cellular lysates treated with OSMI or TMG. Immunoblots with *O*-GlcNAc antibodies revealed that
67 TMG treatment increases *O*-GlcNAc of DNMT1 while OSMI treatment decreases *O*-GlcNAc
68 (Figure 1—figure supplement 1). In addition to Hep3B cells, we found that DNMT1 is *O*-
69 GlcNAcylated in HepG2 cells (Figure 1—figure supplement 2) and B cell derived lymphocytes,
70 indicating DNMT1 is *O*-GlcNAcylated across various cell types (Figure 1—figure supplement 2).
71 To assess the effect of increased glucose metabolism on *O*-GlcNAcylation of DNMT1, we
72 treated Hep3B cells with normal, or low concentrations of glucose (5 mM) or high glucose (25
73 mM) and examined global protein *O*-GlcNAcylation as well as the *O*-GlcNAcylation of DNMT1
74 specifically (Hardiville et al., 2020). Consistent with previous reports (Andrews et al., 2000), the
75 total amount of protein *O*-GlcNAcylation was increased with high glucose treatment (Figure 1A).
76 Global protein *O*-GlcNAcylation was also induced with high concentrations of sucrose, albeit to a
77 lower extent than with glucose (Figure 1—figure supplement 3). To specifically assess the level
78 of *O*-GlcNAcylated DNMT1, we performed immunoprecipitation of DNMT1 from lysates of glucose
79 treated Hep3B cells and immunoblotted for *O*-GlcNAc. As with the analysis of total protein, high
80 glucose treatment increased the *O*-GlcNAcylation of DNMT1 (Figure 1B). High sucrose treatment
81 increased the *O*-GlcNAcylation of DNMT1 as well (Figure 1—figure supplement 3). High glucose
82 and sucrose treatment increased the *O*-GlcNAcylation of DNMT1 in HepG2 cells as well (Figure
83 1—figure supplement 3). The enzymatic activity of OGT or OGA was not significantly changed by
84 glucose treatment (Figure 1—figure supplement 4), consistent with previous results (Seo et al.,
85 2016).
86 To examine whether an increase of *O*-GlcNAcylation of DNMT1 also occurs in primary
87 cells, we collected peripheral blood mononuclear cells (PBMCs) from three separate patient
88 donors and treated the PBMCs with increasing glucose levels (0mM, 5mM, 10mM, 15mM, and

89 20mM). Consistent with our observations in Hep3B cells, we observed an increase in *O*-
90 GlcNAcylation of DNMT1 with increased glucose (Figure 1C). Combining the high glucose
91 condition with OGA inhibition by Thiamet-G (TMG) resulted in a further increase in *O*-
92 GlcNAcylation of DNMT1 (Figure 1—figure supplement 5). To examine the relationship between
93 glucose levels and the *O*-GlcNAcylation of DNMT1 in an *in vivo* context, we examined liver
94 samples from C57BL/6J mice fed an obesogenic high-fat/high-sucrose (HF/HS) diet for 16 weeks
95 (Tang et al., 2020) (details in Methods). These samples displayed an increase in total *O*-
96 GlcNAcylation in liver samples from HF/HS fed mice (Figure 1D) as well as increased *O*-
97 GlcNAcylation of DNMT1 (Figure 1E). These data validate the *O*-GlcNAcylation of DNMT1 and
98 that the degree of *O*-GlcNAcylation of DNMT1 increases with glucose concentrations.
99

100 **Identification of the major *O*-GlcNAcylation sites of DNMT1**

101 To begin to identify the major residues *O*-GlcNAcylated on DNMT1, we utilized OGTSite (Kao et
102 al., 2015) to predict potential sites of *O*-GlcNAcylation. OGTSite, which uses experimentally
103 verified *O*-GlcNAcylation sites to build models of substrate motifs, identified 16 candidate *O*-
104 GlcNAc modified sites on human DNMT1 (Table S1). We next employed mass spectrometry
105 analysis to examine the post-translational modifications on DMNT1 in Hep3B cells. We
106 overexpressed DNMT1 using Myc-tagged DNMT1 construct to increase the protein level of
107 DNMT1 in Hep3B cells (Li et al., 2006). Immunoblots with Myc antibody (Yompakdee et al., 1996)
108 revealed a band corresponding to Myc-DNMT1 in transfected, but not mock transfected, cells
109 (Figure 2—figure supplement 1). We further confirmed with immunoprecipitation followed by
110 immunoblot that the overexpressed Myc-DNMT1 can be *O*-GlcNAcylated (Figure 2—figure
111 supplement 1). For mass spectrometry analysis, we treated Myc-DNMT1 expressing cells with
112 25mM Thiamet-G (TMG) to further increase the *O*-GlcNAcylation of DNMT1. Myc-DNMT1 was
113 enriched from transfected cells by monoclonal Ab-crosslinked immunoprecipitation and subjected
114 to in-solution digestion using three different enzymes (AspN, chymotrypsin, and LysC) and high-

115 resolution LC-MS/MS analysis. Peptide analyses revealed that S878, which is located on the
116 bromo-associated homology (BAH1) domain of DNMT1 is *O*-GlcNAcylated (Figure 2A, B, Figure
117 2—figure supplement 2 and Table S2). In addition, eight unreported phosphorylated residues
118 were newly detected (T208, S209, S873, S874, S953, S954, S1005, and S1202) (Table S2).
119 We chose the three top candidates based on prediction score (T158, T616, and T882) as
120 well as the site identified from mass spectrometry analysis (S878) for further analysis with alanine
121 mutation experiments. The threonine/serine residues were mutated to alanine residues on the
122 Myc-DNMT1 construct and *O*-GlcNAcylation was evaluated with immunoblot following
123 immunoprecipitation. Loss of threonine and serine at positions T158 and S878 respectively
124 resulted in a loss of *O*-GlcNAcylation, indicating that these two residues are required for *O*-
125 GlcNAcylation, with the DNMT1-S878A and DNMT1-T158A/S878A mutant resulting in > 50%
126 reduction of *O*-GlcNAcylation (Figure 2C and Figure 2—figure supplement 3). These results
127 indicate that T158 (near the PCNA binding domain) and S878 (within the BAH1 domain) are the
128 *O*-GlcNAcylated residues of DNMT1.
129
130 ***O*-GlcNAcylation of DNMT1 results in loss of DNA methyltransferase activity**
131 The BAH domains of DNMT1 are known to be necessary for DNA methyltransferase activity
132 (Gong et al., 2021; Yarychkivska et al., 2018). Given that S878 is in the BAH1 domain, we
133 reasoned that *O*-GlcNAcylation of this residue could impact the DNA methyltransferase activity of
134 DNMT1. To test this, we treated Hep3B and HepG2 cells with either low (5mM, CTRL) or high
135 glucose combined with TMG (25mM, *O*-GlcNAc) and evaluated the DNA methyltransferase
136 activity of immunoprecipitated DNMT1 with the EpiQuik DNMT Activity/Inhibition ELISA Easy Kit
137 (EpiGentek, details in Methods). Intriguingly, high glucose combined with TMG treatment reduced
138 the activity of DNMT1 (Figure 3A and Figure 3—figure supplement 1).
139 We next examined the impact of glucose levels on the function of DNMT1 in primary cells
140 by treating PBMCs with increasing concentrations of glucose (0mM, 5mM, 10mM, 15mM, 20mM

141 and 25mM with Thiamet-G) for 96 hours and measuring the DNA methyltransferase activity of
142 DNMT1. We observed a striking dose-dependent inhibition of the DNA methyltransferase activity
143 of DNMT1 (Figure 3B). Lastly, we examined the activity of DNMT1 in the liver samples of mice
144 fed a HF/HS diet, which showed a decreased activity of DNMT1 (Figure 3C) compared to chow
145 fed mice. Together, these data indicate that elevated levels of extracellular glucose can inhibit the
146 methyltransferase function of DNMT1.

147 We next examined the ability of the DNMT1 alanine mutants (DNMT1-T158A and DNMT1-
148 S878A), which cannot be *O*-GlcNAcylated, to attenuate the impact of high glucose- and TMG-
149 induced loss of DNA methyltransferase activity. Compared to the DNA methyltransferase activity
150 of DNMT1-WT (Myc-DNMT1-WT), the DNA methyltransferase activity of DNMT1-S878A (Myc-
151 DNMT1-S878A) is not inhibited by high glucose treatment (Figure 3D), indicating *O*-GlcNAcylation
152 of DNMT1-S878 is directly involved in the inhibition of methyltransferase activity. In contrast, the
153 DNA methyltransferase activity of DNMT1-T158A (Myc-DNMT1-T158A) is inhibited by high
154 glucose combined with TMG treatment in a manner similar to DNMT1-WT (Myc-DNMT1-WT),
155 indicating that *O*-GlcNAcylation of DNMT1-T158 does not affect its DNA methyltransferase
156 activity (Figure 3D).

157 A previous phospho-proteomic analysis revealed that DNMT1-S878 can be
158 phosphorylated (Zhou et al., 2013), but the functional consequences of this have not been
159 investigated. To evaluate the potential that phosphorylation, rather than *O*-GlcNAcylation, of S878
160 is leading to the loss of DNA methyltransferase activity, we generated DNMT1-S878D mutant, a
161 phosphomimetic mutant that cannot be *O*-GlcNAcylated and examined DNA methyltransferase
162 activity in normal and high glucose conditions. This phospho-mimetic mutant did not have loss of
163 DNA methyltransferase activity under high glucose conditions, indicating that *O*-GlcNAcylation of
164 S878 but not phosphorylation of S878 is leading to loss of methyltransferase activity of DNMT1
165 (Figure 3D).

166

167 ***O*-GlcNAcylation of DNMT1 results in subsequent loss of DNA methylation**

168 Given our observations that *O*-GlcNAcylation of DNMT1 inhibits its DNA methyltransferase
169 activity, we reasoned that this would further result in a general loss of DNA methylation. To begin
170 to assess this, DNA methylation was assayed using the global DNA methylation LINE-1 kit (Active
171 Motif, details in Methods) as a proxy for global methylation. Comparison of DNA methylation levels
172 under high glucose and TMG with a DNA methylation inhibitor (5-aza; details in Methods)
173 revealed that high glucose leads to a loss of DNA methylation in a manner comparable with the
174 DNA methylation inhibitor (Figure 3E). This methylation loss was not apparent in the DNMT1-
175 S878A mutant, further demonstrating that *O*-GlcNAcylation of S878 within DNMT1 directly affects
176 DNA methylation under high glucose conditions (Figure 3E and Figure 3—figure supplement 2).
177 A complementary assessment of DNA methylation using methylation sensitive restriction
178 enzymes and gel electrophoresis (details in Methods) revealed similar trends (Figure 3—figure
179 supplement 3).

180

181 ***O*-GlcNAcylation of DNMT1 results in loss of DNA methylation at partially methylated**
182 **domains (PMDs)**

183 To more thoroughly examine the impact of high glucose induced *O*-GlcNAcylation of DNMT1 on
184 the epigenome, Myc-DNMT1 overexpressed cell lines (DNMT1-WT and DNMT1-S878A) were
185 treated with either low (5mM, CTRL) or high glucose combined with TMG (25mM, *O*-GlcNAc) and
186 DNA methylation was profiled with nanopore sequencing (ONT PromethION; details in Methods).
187 Comparison of the methylation profiles in these cells revealed a global loss of methylation in high
188 glucose compared to control (Figure 4A, B and Figure 4—figure supplement 1). Conversely, for
189 the DNMT1-S878A mutant, there was no appreciable decrease in DNA methylation by high
190 glucose (Figure 4A). These results collectively indicate that *O*-GlcNAcylation of S878 of DNMT1
191 leads to a global loss of DNA methylation.

192 Examination of DNA methylation changes induced by *O*-GlcNAcylation of DNMT1
193 revealed a preferential loss of DNA methylation at liver cancer PMDs (Li et al., 2016) that was not
194 observed in S878A mutant cells (Figure 4B and C). Partially methylated domains (PMDs) have
195 several defining features, including being relatively gene poor and harboring mostly lowly
196 transcribed genes (Decato et al., 2020). We stratified the genome in terms of gene density and
197 transcription rate (see Methods for details) and found that regions that lose methylation in high
198 glucose conditions are largely gene poor (Figure 4D) and contain lowly transcribed genes (Figure
199 4E) (Chang et al., 2014). PMDs have furthermore been linked to regions of late replication
200 associated with the nuclear lamina (Brinkman et al., 2019). We therefore examined the correlation
201 between loss of methylation caused by high glucose and replication timing (Thurman et al., 2007).
202 In DNMT1-WT cells, late replication domains preferentially lose DNA methylation in high
203 glucose/TMG conditions compared to early replication domains (Figure 4F). This loss of
204 methylation was not observed in DNMT1-S878A mutant cells (Figure 4—figure supplement 2).
205

206 **Evolutionarily young transposable elements (TEs) are protected from loss of methylation**
207 **in high glucose conditions**

208 One of the major functions of DNA methylation in mammalian genomes is the repression of
209 repetitive elements (Edwards et al., 2017). Furthermore, it has been shown that many chromatin
210 proteins involved in the repression of transposable elements (TEs) are capable of being *O*-
211 GlcNAcylated (Boulard et al., 2020). We therefore examined the potential of *O*-GlcNAcylation of
212 DNMT1 to lead to loss of suppression of TEs. We found that high glucose conditions resulted in
213 methylation loss at TEs in a manner similar to the non-repetitive fraction of the genome (Figure
214 4—figure supplement 3), with a more dramatic loss of methylation at LINEs and LTRs as
215 compared to SINE elements (Figure 4—figure supplement 3). Given that evolutionarily recent TEs
216 are more likely to lose methylation than older elements in a variety of systems (Almeida et al.,
217 2022; Zhou et al., 2020), we examined the methylation status of two younger subfamilies, LTR12C

218 (*Hominoidea*) and HERVH-int (*Catarrhini*) elements (Figure 4—figure supplement 4). While
219 HERVH-int elements show a loss of methylation similar to the rest of the genome, LTR12C
220 elements do not lose methylation in the same manner (Figure 4—figure supplement 4) suggesting
221 they are protected from the loss of methylation. To identify the possible regulatory mechanisms
222 behind the continued maintenance of methylation of LTR12C, an analysis was performed on all
223 LTR12C's present within hepatic cancer PMDs relative to ChIP-exo data of KRAB-associated
224 zinc-finger proteins, a family of proteins associated with the regulation of transposons. ZFP57 and
225 ZNF605 (on top of the previously defined ZNF676) demonstrate binding to a significant number
226 of LTR12C elements present in liver cancer PMDs (Figure 4—figure supplement 5). Stratifying all
227 TEs by evolutionary age and examining the methylation changes induced by *O*-GlcNAcylation of
228 DNMT1 for each clade revealed that evolutionarily recent elements are less likely to lose
229 methylation (Figure 4—figure supplement 6).
230
231 **Methylation changes at promoter regions of apoptosis and oxidative stress response**
232 **genes upon inhibition of DNMT1**
233 To further examine the impact of the altered epigenome in high glucose conditions, we examined
234 the methylation levels of promoter regions (defined as the 2kb window upstream and downstream
235 of the transcription start site (TSS)) (Figure 4—figure supplement 1 and Figure 5—figure
236 supplement 1). Hypermethylated (gain of methylation) and hypomethylated (loss of methylation)
237 genes were classified as genes with differentially methylated regions overlapping the promoters
238 (Figure 5—figure supplement 1). Pathway analysis (see Methods for details) revealed that genes
239 with hypomethylated promoters are involved in apoptosis and oxidative stress response pathways
240 (Figure 5—figure supplement 2). Examination of apoptosis replated proteins using an apoptosis
241 proteome array revealed that apoptosis agonist proteins (cleaved-caspase3 and phopho-p53
242 (S15)) are increased and antagonistic proteins (pro-caspase3, surviving, and claspin) are
243 decreased by high glucose treatment (Figure 5—figure supplement 3). Intriguingly, only cIAP-1

244 protein is increased in the high glucose treated DNMT1-S878A mutant cells (Figure 5—figure
245 supplement 3).
246
247 **DNA hypomethylation induced DNA damage and triggers apoptosis by high glucose**
248 High glucose induced generation of reactive-oxygen-species (ROS) has been shown to result in
249 increased cell death (Allen et al., 2005). Increased ROS has furthermore been shown to result in
250 upregulation of DNMT1 (He et al., 2012; O'Hagan et al., 2011). To further explore the link between
251 glucose levels, DNMT1 and cell death, we treated DNMT1-WT and DNMT1-S878A cells with
252 either low or high glucose combined with TMG for 96 hours and examined the fluorescence of
253 2′,7′-dichlorofluorescein diacetate (DCFH-DA) as an indicator for ROS (Figure 5A). The levels of
254 ROS were increased upon treatment with 25 mM glucose with TMG in both of DNMT1-WT and
255 DNMT1-S878A (Figure 5A). Given that high levels of ROS can lead to increased DNA damage
256 and subsequent cell death (Rowe et al., 2008), we analyzed 8-hyrdoxy-2'deoxyguanosine (8-
257 OHdG) as a marker for oxidative DNA damage using EpiQuik 8-OHdG DNA damage
258 quantification kit (EpiGentek, details in Methods). Interestingly, DNA damage was reduced in high
259 glucose treated DNMT1-S878A cells as compared to WT cells (Figure 5B). Furthermore, DNA
260 damage induced by low glucose with 5-aza treatment suggests that DNA hypomethylation is
261 associated with increased DNA damage (Figure 5B) (Palii et al., 2008). Finally, examination of
262 propidium Iodide (PI) levels revealed that cell death was prominently increased in the high glucose
263 treated in DNMT1-WT cells but suppressed in the DNMT1-S878A mutants (Figure 5C). Taken
264 together, these results suggest that ROS-induced DNA damage under hyperglycemic conditions
265 is mitigated by DNA methylation; when DNMT1 function is inhibited via *O*-GlcNAcylation and
266 methylation is lost, ROS-induced DNA damage increases, resulting in apoptosis. These results
267 indicate a that extracellular metabolic stress and cell fate are linked through epigenetic regulation.
268
269

Discussion

Although there is a great deal of evidence regarding the important regulatory role of *O*-GlcNAcylation in gene regulation (Brimble et al., 2010), a direct link with DNA methylation has not previously been established. The maintenance methyltransferase DNMT1 is essential for faithful maintenance of genomic methylation patterns and mutations in DNMT1, particularly in the BAH domains, lead to disruption of DNA methylation (Yarychkivska et al., 2018). While it has been shown that DNTM1 can be *O*-GlcNAcylated (Boulard et al., 2020), the site of *O*-GlcNAc modification on DNMT1 as well as the functional consequences of this modification have not previously been examined.

We reveal that *O*-GlcNAcylation of DNMT1 impacts its DNA methyltransferase activity and affects DNMT1 function leading to loss of DNA methylation at partially methylated domains (PMDs). PMDs are observed in both healthy and cancerous cells and have been suggested to be associated with mitotic dysfunction. However, models for how these domains are established remain incomplete (Decato et al., 2020). The results presented here suggest an additional layer whereby *O*-GlcNAcylation of DNMT1 at S878 due to increased glucose levels can inhibit the function of DNA methyltransferase activity of DNMT1, resulting in loss of methylation and establishment of partially methylated domains.

High glucose conditions have previously been reported to lead to an increase in nuclear 25-Hydroxycholesterol, which induces lipid accumulation and activates DNMT1 (Allen et al., 2005; Wang et al., 2020). Our results are consistent with the activity of DNMT1 gradually increased by glucose concentrations (Figure 3—figure supplement 1). This trend is reversed, however, upon TMG treatment (Figure 3—figure supplement 1), suggesting that the increased activity of DNMT1 associated with glucose treatment is directly inhibited by *O*-GlcNAcylation within DNMT1.

Metabolic diseases such as obesity and diabetes have been linked to epigenetic changes that alter gene regulation (Ling and Ronn, 2019). It has previously been established that there is a general increase in protein *O*-GlcNAcylation in hyperglycemia conditions (Vasconcelos-Dos-

296 Santos et al., 2018) and several epigenetic regulatory factors have been shown to have increased
297 *O*-GlcNAcylation under high glucose conditions (Bauer et al., 2015; Etchegaray and
298 Mostoslavsky, 2016; Yang et al., 2020). Our findings that extracellular glucose promotes *O*-
299 GlcNAcylation of DNMT1 and inhibition of DNMT1's function in maintenance of genomic
300 methylation provide direct evidence that extracellular levels of glucose is linked with epigenomic
301 regulation.
302
303 **Materials and Methods**
304 **Antibodies and Regents**
305 Information on antibodies and reagents used in this study are provided in Table S3.
306
307 **Cell culture and plasmid DNA transfection**
308 Human hepatocellular carcinoma cell lines HepG2 (HB-8065), and Hep3B (HB-8064) were
309 purchased from ATCC (Manassas, VA, USA). All cell lines were shown to be negative in
310 mycoplasma test using MycoScope (MY01050, Genlantis, San Diego, CA, USA). The following
311 ATCC-specified cell culture media were used: Dulbecco's modified Eagle's medium (DMEM,
312 11885-084, Grand Island, NY, USA) or high glucose Dulbecco's modified Eagle's medium
313 (DMEM, 11995-065, Gibco, Grand Island, NY, USA) with 10% fetal bovine serum (FBS,
314 SH30910.03, HyClone, South Logan, UT, USA) and Opti-MEM (1869048, Gibco, Grand Island,
315 NY, USA). All cells were cultured in a 37°C with a 5% CO_2 atmosphere incubator. HepG2 and
316 Hep3B cells were transiently transfected (with the pcDNA3 with or without DNMT1 cDNA) using
317 Lipofectamine 3000 (Invitrogen, Carlsbad, CA, USA) and selected with Geneticin (G418, 10131-
318 035, Gibco, Grand Island, NY, USA) according to the manufacturer's instructions. Human DNMT1
319 plasmid was purchased from Addgene (#36939, Watertown, MA, USA) (Li et al., 2006).
320
321

322 **Isolation of peripheral blood mononuclear cells (PBMCs)**

323 Blood samples from de-identified healthy donors were obtained following guidelines at the City of
324 Hope as describe (Leung et al., 2018). PBMCs such as lymphocyte, monocyte or a macrophage
325 were isolated directly from human whole blood using Ficoll-Paque (Premium, GE Healthcare,
326 Chicago, IL, USA) density gradient centrifugation. 15ml whole blood was mixed with same volume
327 of phosphate-buffered saline containing 0.1% Fetal bovine serum + 2mM EDTA (PBS solution).
328 Next, the blood mix was placed on top of 15 ml Ficoll and centrifuged at 400g to 200g for 40 min
329 without brake. Next, remove the supernatant and washed three times with PBS solution.

330

331 **Isolation of B cells and Epstein-Barr virus (EBV) infection for lymphocyte transformation**

332 $CD19^+$ B cells were isolated from PBMCs (peripheral blood mononuclear cells) using Dynabeads
333 $CD19^+$ pan B (11143D, Invitrogen, Carlsbad, CA, USA) according to the manufacturer's
334 instruction. 2.5 x 10^8 cells of PBMCs were resuspended in 10ml Isolation buffer (PBS, 0.1% BSA,
335 2mM EDTA). 250 µl of pre-washed beads were added to PBMCs and incubated for 20 min in 4°C
336 with gentle rotation. For positive isolation of $CD19^+$ B cells, beads and supernatant were
337 separated using magnet, and supernatant was discarded. Beads were washed three times, and
338 beads bounded with $CD19^+$ B cells were resuspended with 2.5 ml of cell culture medium (80%
339 RPMI1640, 20 % heat-inactivated FBS, Glutamine). $CD19^+$ B cells were released from
340 Dynabeads using DETACHaBEAD (Invitrogen, ca12506D) according to the manufacturer's
341 instruction.

342 B cells were infected with Epstein-Barr virus (EBV) to transform lymphocyte. 10 ml of B
343 cells were transferred into T75 flask. 1.5ml of stock EBV collected from a B95-8 strain-containing
344 marmoset cell lines and 1ml of Phytohemagglutinin P (PHA-P) were added to flask and incubated
345 in a 37°C with a 5% CO_2 atmosphere incubator. Every 5 to 7 days, 10 ml of cell culture medium
346 was added. Cells were let to grow in CO_2 atmosphere incubator for 30 days until all B cells were
347 transformed to LCL.

348 **Mouse liver samples**

349 All animal experiments conducted have been approved by the Institutional Animal Care and Use
350 Committees at City of Hope. All of the animals were handled according to approved institutional
351 animal care and use committee (IACUC) protocols (#17010). C57BL/6J mice were randomized
352 to receive irradiated high-fat / high-sucrose (HF/HS) diet (D12266Bi, Research Diets Inc, 17%
353 kcal protein, 32% kcal fat, 51% kcal carbohydrate) starting at 8 weeks old for 16 weeks. Mice on
354 chow diet (D12489Bi, Research Diets Inc, 16.4% kcal protein, 70.8% kcal carbohydrate, 4.6%
355 kcal fat) were fed for the same duration. To reduce blood contamination, mice were washed 10x
356 with phosphate-buffered saline (PBS) solution. Washed liver tissues (two CHOW and two HF/HS)
357 were cut into several pieces and divided into three groups each (three sets per each condition,
358 total 12 samples). Each group of washed liver tissues were lysed with non-detergent IP buffer in
359 the presence of a protease inhibitor (Cat#8340; Sigma-Aldrich) and a phosphatase inhibitor
360 cocktail (Cat# 5870; Cell Signaling) for the western blotting or immunoprecipitation. An increase
361 in fasting blood glucose levels due to the HF/HS diet has been previously reported (Franson et
362 al., 2021; Tang et al., 2020). At the end points, mice were euthanized with CO2 inhalation.

363

364 **Immunoprecipitation and western blot analysis**

365 Cell lysates were incubated with specific antibodies and lysis buffer for 4 hours. Subsequently, 30
366 µl of washed Dynabeads (14311D, Thermo Fisher, Waltham, MA, USA) were added to each
367 lysate and incubated overnight at 4°C. Next, the beads were washed five times, and the antigens
368 were eluted twice using 8M Urea buffer (8M Urea, 20mM Tris pH 7.5, and 100mM NaCl) and
369 concentrated. The resulting samples were separated by Mini-PROTEAN TGX (4-20%, 4561093,
370 Bio-Rad Laboratories, Hercules, CA, USA) and transferred onto nitrocellulose membranes
371 (Amersham Hybond, 10600021, GE Healthcare, Chicago, IL, USA) using Trans-Blot SD Semi-
372 dry Transfer Cell system (Bio-Rad Laboratories, Hercules, CA, USA). The membranes were then
373 blocked with 5% skim milk in Tris-buffered saline + Tween-20 (TBS-T; 20 mM Tris, 137 mM NaCl,

374 0.1% Tween-20, pH 7.6), incubated overnight at 4°C with a 1:1000 dilution of each antibodies,
375 and subsequently incubated for 1 h with a 1:5000 dilution of a horseradish peroxidase–conjugated
376 goat anti-mouse secondary antibody (ab6789, Abcam, Cambridge, UK) or goat anti-rabbit
377 secondary antibody (ab6721, Abcam, Cambridge, UK). Immunoreactive proteins were detected
378 using SuperSignal West Dura Extended Duration Substrate (34076, Thermo, Rockford, IL, USA)
379 and detected using a ChemiDoc MP Imaging system (Bio-Rad Laboratories, Hercules, CA, USA).
380 The band intensity was densitometrically evaluated using Image Lab software (Version 5.2, Bio-
381 Rad Laboratories, Hercules, CA, USA).
382
383 **Protein identification using the Thermo Fusion Lumos system LC-MS/MS**
384 LC-MS separation was performed on an Thermo Fusion Lumos system (Thermo Scientific,
385 Waltham, MA, USA). For LC separation, 60-minute LC gradient on EasySpray column (particle
386 sizes: 500 mm, 75 μm) was used for peptide separation. Mass spectra for peptide identification
387 or quantification were acquired using an Orbitrap Lumos mass at 120,000 resolutions. Full MS
388 scan ranges were acquired from 156 to 2000 m/z. MS/MS spectra were acquired at a resolution
389 of 30,000 using HCD at 35% collision energy.
390 Identify post-translational modifications on DNMT1 using complementary in-solution
391 digestion with three enzymes (chymotrypsin, AspN and LysC). Protein was reduced with DTT and
392 alkylated with iodoacetamide. Aliquots of protein were separately digested with three enzymes
393 and peptides were desalted using a C18 tip.
394 Raw data files were submitted to Byonic (v2.16.11) for target decoy search against the
395 human protein database (uniprot/swissprot, 2020). Peptide-level confidence threshold was set at
396 99% (FDR <0.01). The sample was bracketed by *E. coli* QC runs, which were then correlated to
397 ensure instrument quality. QC passed threshold (≥ 0.9) with an R^2 of 0.98 (correlation value,
398 R=0.99)
399

400 **Site-directed point mutation**

401 Specific primers for serine (S) and threonine (T) to alanine (A) and aspartic acid (D) mutations of
402 DNMT1 were designed and used to site-directed point mutations in a plasmid vector. A
403 recombinant DNA pcDNA3/Myc-DNMT1 was a gift from Arthur Riggs (Addgene plasmid #36939
404 Watertown, MA, USA) (Li et al., 2006). A PCR-amplified DNA fragment of pcDNA3-DNMT1 was
405 generated using Q5 Site-Directed Mutagenesis Kit (E0554S, NEB, Ipswich, MA, USA). The
406 primers used in this process are described in Supporting Information. After PCR, the non-mutated
407 sequences were cleaved using Q5 KLD enzyme (New England Biolabs, Ipswich, MA, USA)
408 according to the manufacturer's instructions. The mutated vectors were transformed into *E. coli*
409 competent cells (NEB 5-alpha, New England Biolabs, Ipswich, MA, USA) that were cultured and
410 prepared using a GenElute HP Plasmid Midi kit (NA0200-1KT, Sigma-Aldrich, St. Louis, MO).

411

412 **DNA methyltransferase activity assay**

413 DNA methyltransferase activities of endogenous DNMT1 and recombinant DNMT1 were
414 measured by EpiQuik DNMT Activity/Inhibition ELISA Easy Kit (P-3139-48, EpiGentek,
415 Farmingdale, NY, USA) according to the manufacturer's instructions. The endogenous DNMT1
416 (by anti-DNMT1 Ab, 60B1220.1) and recombinant DNMT1 (by anti-Myc, ab18185) were enriched
417 using immunoprecipitation from each cell or tissue lysates. DNMT1s were isolated and normalized
418 by BCA analysis. The activity of 5 ng DNMT1 was analyzed by 450nm ELISA with an optimal
419 wavelength of 655nm.

420

421 **Global DNA Methylation LINE-1 assay**

422 Global DNA methylation LINE-1 were measured by Active Motif (55017, Carlsbad, CA, USA)
423 according to the manufacturer's instructions. Each Hep3B and myc-DNMT1 overexpressed
424 mutants (DNMT1-WT or DNMT1-S878A) were treated 5mM glucose, or 25mM glucose, and 5-

425 aza (negative control). The activity of 100 ng was analyzed by 450nm ELISA with an optimal
426 wavelength of 655nm.
427
428 **Agilent 4200 TapeStation**
429 Global DNA methylation were measured by Agilent 4200 TapeStation system (Santa Clara, CA,
430 USA) with the Genomic DNA ScreenTape (5064-5365) and Genomic DNA Reagent (5067-5366)
431 according to the manufacturer's instructions.
432
433 **Nanopore PromethION sequencing**
434 Genomic DNA was isolated from each DNMT1-WT or DNMT1-S878A treated 5mM glucose or
435 25mM glucose combined with TMG using the QIAGEN DNA Mini Kit (13323, Qiagen) with
436 Genomic-tip (10223, Qiagen) according to the manufacturer's instructions. Sequencing libraries
437 were prepared using Ligation sequencing kit (SQK-LSK109, Oxford Nanopore Technologies)
438 according to the manufacturer's instructions. Sequencing was performed on a PromethION
439 (Oxford Nanopore Technologies). Data indexing were performed using nanopolish
440 (RRID:SCR_016157). Reads were aligned using minimap2 (RRID:SCR_018550) with the options
441 -a -x map-ont (Li, 2018). Methylation state of CpGs was called using nanopolish
442 (RRID:SCR_016157) with the options call-methylation -t 8 (Loman et al., 2015). Only loci with
443 greater than 5x coverage were retained for analysis, comprising 90% of CpGs in the genome
444 (Figure 4—figure supplement7) . Methylation percentage was averaged across CpG islands.
445
446 **Determination of gene-poor or gene-rich regions and FPKM**
447 Hep3B RNA-seq data were obtained from a previous publication (Chang et al., 2014). Fastq files
448 were aligned using HISAT2 version 2.1.0 (RRID:SCR_015530) to the hg19 genome. Duplications
449 are removed using picard version 2.10.1 (RRID:SCR_006525). Aligned reads were sorted using
450 samtools version 1.10 (RRID:SCR_002105). UCSC genome browser tracks were established

451 using bedGraphToBigWig. FPKM was calculated using StringTie version 1.3.4d
452 (RRID:SCR_016323).
453 For all datasets, Bedgraph files were generated using bedtools version 2.29.0
454 (RRID:SCR_006646). BigWigs were generated using the UCSCtools bedGraphToBigWig.
455 Heatmap of global DNA methylation for DNMT1-WT and DNMT1-S878A cells under low or high
456 glucose were generated using a custom script to profile the read coverage at each base and were
457 visualized using pheatmap version 1.0.12 (RRID:SCR_016418). All other heatmaps and
458 aggregate plots of loci that extend were generated using deeptools (RRID:SCR_016366).
459

460 **Measurement of Reactive Oxygen Species (ROS) and Propidium Iodide (PI) staining**

461 DNMT1-WT and DNMT1-S878A cells were seeded into 12-well plates with 5mM or 25mM glucose
462 and TMG. The medium in each well was replaced with HBSS with 10 μM DCF-DA (2′,7′-
463 dichlorofluorescein diacetate; D6883, Abcam) or propidium iodide staining solution (P4864,
464 Abcam). The fluorescence was filtered with fluorescein isothiocyanate (FITC) for ROS or Texas
465 Red for PI staining (Shin et al., 2020). Averages of fluorescence were analyzed by Olympus
466 Cellsens software.
467

468 **DNA damage analysis**

469 DNA damage was analyzed using EpiQuik 8-OHdG DNA Damage Quantification Direct Kit (P-
470 6003, EpiGentek) according to the manufacturer's protocol. The activity of 200 ng DNA was
471 analyzed by 450nm absorbance microplate reader.
472

473 **Apoptosis array analysis**

474 Apoptosis related proteins were analyzed using Proteome profiler human apoptosis array kit
475 (ARY009, R&D Systems) according to the manufacturer's protocol. The spots were detected
476 using a ChemiDoc MP Imaging system (Bio-Rad Laboratories, Hercules, CA, USA) (Na et al.,

477 2020). The band intensity was densitometrically evaluated using Image Lab software (Version
478 5.2, Bio-Rad Laboratories, Hercules, CA, USA).
479
480 **KZFP binding in PMD-associated LTR12Cs**
481 A list of partially methylated domains (PMD) in Hep3B cells were obtained from a previous
482 publication (Li et al., 2016). A full list of LTR12Cs was generated from filtering hg19-repmask.bed.
483 The PMD-associated LTR12Cs were found using bedtools version 2.29.0 (RRID:SCR_006646).
484 Putative KZFP regulators of LTR12Cs were determined using the consensus sequence of
485 LTR12Cs and ChIP-exo from the Imbeault and Trono studies on the UCSC Repeat Browser
486 (Imbeault et al., 2017). PMD-associated LTR12Cs were then aligned again with peak files
487 containing the ChIP-exo data to acquire a list of PMD-associated LTR12Cs with KZFP binding.
488 Significant binding was defined as > 5 sequences bound, as most LTR12Cs demonstrated very
489 minimal KZFP binding (< 1 sequences bound).
490
491 **Quantification and Statistical Analysis**
492 Statistical analyses were performed and graphed using GraphPad Prism 9 (v9.3.1). All statistical
493 tests were performed by three independent experiments assay, and the data are presented as
494 means ± standard deviations. *$p < 0.001$; **$p < 0.0005$; ***$p < 0.0001$ by Student's *t*-test; ns, not
495 significant; Data are represented as mean ± SD.
496
497 **Acknowledgements**
498 This manuscript is dedicated to the memory of Dr. Arthur Riggs. This work was supported by the
499 National Institutes of Health, grants R01DK112041 and R01CA220693 (D.E.S.). Research
500 reported in this publication included work performed in the Pathology and Integrative Genomics
501 Cores of the City of Hope and was supported by the City of Hope CCSG Pilot award from National
502 Cancer Institute of the National Institutes of Health under award number P30CA033572.

503 **Competing interest**

504 The authors declare no competing interest.

505

506 **Data availability**

507 PromethION sequencing data have been deposited in the NCBI Gene Expression Omnibus (GEO)

508 and Sequence Read Archive (SRA) under accession no. GSE201470.

509

510 **Author Contributions**

511 Heon Shin, Conceptualization, Data curation, Formal analysis, Investigation, Methodology,

512 Validation, Visualization, Writing – original draft, Writing – review and editing; Amy Leung,

513 Conceptualization, Formal analysis, Methodology; Kevin R. Costello, Data curation, Formal

514 analysis; Parijat Senapati, Hiroyuki Kato, Michael Lee, Dimitri Lin, Formal analysis; Xiaofang

515 Tang, Formal analysis, Provide samples; Zhen Bouman Chen, Provide samples; Dustin E.

516 Schones, Conceptualization, Funding acquisition, Investigation, Methodology, Project

517 administration, Supervision, Writing – original draft, Writing – review and editing.

518

519 **References**

520 Allen, D.A., Yaqoob, M.M., and Harwood, S.M. (2005). Mechanisms of high glucose-induced
521 apoptosis and its relationship to diabetic complications. J Nutr Biochem *16*, 705-713.
522 Almeida, M.V., Vernaz, G., Putman, A.L.K., and Miska, E.A. (2022). Taming transposable
523 elements in vertebrates: from epigenetic silencing to domestication. Trends Genet.
524 Andrews, S.R., Charnock, S.J., Lakey, J.H., Davies, G.J., Claeyssens, M., Nerinckx, W.,
525 Underwood, M., Sinnott, M.L., Warren, R.A., and Gilbert, H.J. (2000). Substrate specificity in
526 glycoside hydrolase family 10. Tyrosine 87 and leucine 314 play a pivotal role in discriminating
527 between glucose and xylose binding in the proximal active site of Pseudomonas cellulosa
528 xylanase 10A. J Biol Chem *275*, 23027-23033.
529 Bauer, C., Gobel, K., Nagaraj, N., Colantuoni, C., Wang, M., Muller, U., Kremmer, E., Rottach,
530 A., and Leonhardt, H. (2015). Phosphorylation of TET proteins is regulated via O-GlcNAcylation
531 by the O-linked N-acetylglucosamine transferase (OGT). The Journal of biological chemistry *290*,
532 4801-4812.
533 Berman, B.P., Weisenberger, D.J., Aman, J.F., Hinoue, T., Ramjan, Z., Liu, Y., Noushmehr, H.,
534 Lange, C.P., van Dijk, C.M., Tollenaar, R.A., et al. (2011). Regions of focal DNA hypermethylation
535 and long-range hypomethylation in colorectal cancer coincide with nuclear lamina-associated
536 domains. Nat Genet *44*, 40-46.

537 Bestor, T.H., and Ingram, V.M. (1983). Two DNA methyltransferases from murine erythroleukemia
538 cells: purification, sequence specificity, and mode of interaction with DNA. Proc Natl Acad Sci U
539 S A *80*, 5559-5563.
540 Boulard, M., Rucli, S., Edwards, J.R., and Bestor, T.H. (2020). Methylation-directed glycosylation
541 of chromatin factors represses retrotransposon promoters. Proceedings of the National Academy
542 of Sciences of the United States of America *117*, 14292-14298.
543 Brimble, S., Wollaston-Hayden, E.E., Teo, C.F., Morris, A.C., and Wells, L. (2010). The Role of
544 the O-GlcNAc Modification in Regulating Eukaryotic Gene Expression. Curr Signal Transduct
545 Ther *5*, 12-24.
546 Brinkman, A.B., Nik-Zainal, S., Simmer, F., Rodriguez-Gonzalez, F.G., Smid, M., Alexandrov,
547 L.B., Butler, A., Martin, S., Davies, H., Glodzik, D., et al. (2019). Partially methylated domains are
548 hypervariable in breast cancer and fuel widespread CpG island hypermethylation. Nat Commun
549 *10*, 1749.
550 Chang, C., Li, L., Zhang, C., Wu, S., Guo, K., Zi, J., Chen, Z., Jiang, J., Ma, J., Yu, Q., et al.
551 (2014). Systematic analyses of the transcriptome, translatome, and proteome provide a global
552 view and potential strategy for the C-HPP. J Proteome Res *13*, 38-49.
553 Chen, Q., Chen, Y., Bian, C., Fujiki, R., and Yu, X. (2013). TET2 promotes histone O-
554 GlcNAcylation during gene transcription. Nature *493*, 561-564.
555 de Jesus, T., Shukla, S., and Ramakrishnan, P. (2018). Too sweet to resist: Control of immune
556 cell function by O-GlcNAcylation. Cell Immunol *333*, 85-92.
557 Decato, B.E., Qu, J., Ji, X., Wagenblast, E., Knott, S.R.V., Hannon, G.J., and Smith, A.D. (2020).
558 Characterization of universal features of partially methylated domains across tissues and species.
559 Epigenetics Chromatin *13*, 39.
560 Edwards, J.R., Yarychkivska, O., Boulard, M., and Bestor, T.H. (2017). DNA methylation and DNA
561 methyltransferases. Epigenetics Chromatin *10*, 23.
562 Elbatrawy, A.A., Kim, E.J., and Nam, G. (2020). O-GlcNAcase: Emerging Mechanism, Substrate
563 Recognition and Small-Molecule Inhibitors. ChemMedChem *15*, 1244-1257.
564 Etchegaray, J.P., and Mostoslavsky, R. (2016). Interplay between Metabolism and Epigenetics:
565 A Nuclear Adaptation to Environmental Changes. Molecular cell *62*, 695-711.
566 Franson, J.J., Grose, J.H., Larson, K.W., and Bridgewater, L.C. (2021). Gut Microbiota Regulates
567 the Interaction between Diet and Genetics to Influence Glucose Tolerance. Medicines (Basel) *8*.
568 Gong, Y., Zhang, X., Zhang, Q., Zhang, Y., Ye, Y., Yu, W., Shao, C., Yan, T., Huang, J., Zhong,
569 J., et al. (2021). A natural DNMT1 mutation elevates the fetal hemoglobin level via epigenetic
570 derepression of the gamma-globin gene in beta-thalassemia. Blood *137*, 1652-1657.
571 Guinez, C., Filhoulaud, G., Rayah-Benhamed, F., Marmier, S., Dubuquoy, C., Dentin, R., Moldes,
572 M., Burnol, A.F., Yang, X., Lefebvre, T., et al. (2011). O-GlcNAcylation increases ChREBP protein
573 content and transcriptional activity in the liver. Diabetes *60*, 1399-1413.
574 Hansen, R.S., Thomas, S., Sandstrom, R., Canfield, T.K., Thurman, R.E., Weaver, M., Dorschner,
575 M.O., Gartler, S.M., and Stamatoyannopoulos, J.A. (2010). Sequencing newly replicated DNA
576 reveals widespread plasticity in human replication timing. Proc Natl Acad Sci U S A *107*, 139-144.
577 Hardiville, S., Banerjee, P.S., Selen Alpergin, E.S., Smith, D.M., Han, G., Ma, J., Talbot, C.C., Jr.,
578 Hu, P., Wolfgang, M.J., and Hart, G.W. (2020). TATA-Box Binding Protein O-GlcNAcylation at
579 T114 Regulates Formation of the B-TFIID Complex and Is Critical for Metabolic Gene Regulation.
580 Mol Cell *77*, 1143-1152 e1147.
581 Hart, G.W., Housley, M.P., and Slawson, C. (2007). Cycling of O-linked beta-N-acetylglucosamine
582 on nucleocytoplasmic proteins. Nature *446*, 1017-1022.
583 Hart, G.W., Kreppel, L.K., Comer, F.I., Arnold, C.S., Snow, D.M., Ye, Z., Cheng, X., DellaManna,
584 D., Caine, D.S., Earles, B.J., et al. (1996). O-GlcNAcylation of key nuclear and cytoskeletal
585 proteins: reciprocity with O-phosphorylation and putative roles in protein multimerization.
586 Glycobiology *6*, 711-716.

587 He, J., Xu, Q., Jing, Y., Agani, F., Qian, X., Carpenter, R., Li, Q., Wang, X.R., Peiper, S.S., Lu,
588 Z., et al. (2012). Reactive oxygen species regulate ERBB2 and ERBB3 expression via miR-
589 199a/125b and DNA methylation. EMBO Rep *13*, 1116-1122.
590 Imbeault, M., Helleboid, P.Y., and Trono, D. (2017). KRAB zinc-finger proteins contribute to the
591 evolution of gene regulatory networks. Nature *543*, 550-554.
592 Ito, R., Katsura, S., Shimada, H., Tsuchiya, H., Hada, M., Okumura, T., Sugawara, A., and
593 Yokoyama, A. (2014). TET3-OGT interaction increases the stability and the presence of OGT in
594 chromatin. Genes Cells *19*, 52-65.
595 Kao, H.J., Huang, C.H., Bretana, N.A., Lu, C.T., Huang, K.Y., Weng, S.L., and Lee, T.Y. (2015).
596 A two-layered machine learning method to identify protein O-GlcNAcylation sites with O-GlcNAc
597 transferase substrate motifs. BMC Bioinformatics *16 Suppl 18*, S10.
598 Leung, A., Trac, C., Kato, H., Costello, K.R., Chen, Z., Natarajan, R., and Schones, D.E. (2018).
599 LTRs activated by Epstein-Barr virus-induced transformation of B cells alter the transcriptome.
600 Genome Res *28*, 1791-1798.
601 Li, H. (2018). Minimap2: pairwise alignment for nucleotide sequences. Bioinformatics *34*, 3094-
602 3100.
603 Li, H., Rauch, T., Chen, Z.X., Szabo, P.E., Riggs, A.D., and Pfeifer, G.P. (2006). The histone
604 methyltransferase SETDB1 and the DNA methyltransferase DNMT3A interact directly and
605 localize to promoters silenced in cancer cells. J Biol Chem *281*, 19489-19500.
606 Li, X., Liu, Y., Salz, T., Hansen, K.D., and Feinberg, A. (2016). Whole-genome analysis of the
607 methylome and hydroxymethylome in normal and malignant lung and liver. Genome Res *26*,
608 1730-1741.
609 Ling, C., and Ronn, T. (2019). Epigenetics in Human Obesity and Type 2 Diabetes. Cell Metab
610 *29*, 1028-1044.
611 Lister, R., Pelizzola, M., Dowen, R.H., Hawkins, R.D., Hon, G., Tonti-Filippini, J., Nery, J.R., Lee,
612 L., Ye, Z., Ngo, Q.M., et al. (2009). Human DNA methylomes at base resolution show widespread
613 epigenomic differences. Nature *462*, 315-322.
614 Loman, N.J., Quick, J., and Simpson, J.T. (2015). A complete bacterial genome assembled de
615 novo using only nanopore sequencing data. Nat Methods *12*, 733-735.
616 Maresca, A., Zaffagnini, M., Caporali, L., Carelli, V., and Zanna, C. (2015). DNA
617 methyltransferase 1 mutations and mitochondrial pathology: is mtDNA methylated? Front Genet
618 *6*, 90.
619 Martin, S.E.S., Tan, Z.W., Itkonen, H.M., Duveau, D.Y., Paulo, J.A., Janetzko, J., Boutz, P.L.,
620 Tork, L., Moss, F.A., Thomas, C.J., et al. (2018). Structure-Based Evolution of Low Nanomolar
621 O-GlcNAc Transferase Inhibitors. J Am Chem Soc *140*, 13542-13545.
622 Na, K., Kim, M., Kim, C.Y., Lim, J.S., Cho, J.Y., Shin, H., Lee, H.J., Kang, B.J., Han, D.H., Kim,
623 H., et al. (2020). Potential Regulatory Role of Human-Carboxylesterase-1 Glycosylation in Liver
624 Cancer Cell Growth. J Proteome Res *19*, 4867-4883.
625 O'Hagan, H.M., Wang, W., Sen, S., Destefano Shields, C., Lee, S.S., Zhang, Y.W., Clements,
626 E.G., Cai, Y., Van Neste, L., Easwaran, H., et al. (2011). Oxidative damage targets complexes
627 containing DNA methyltransferases, SIRT1, and polycomb members to promoter CpG Islands.
628 Cancer Cell *20*, 606-619.
629 Palii, S.S., Van Emburgh, B.O., Sankpal, U.T., Brown, K.D., and Robertson, K.D. (2008). DNA
630 methylation inhibitor 5-Aza-2'-deoxycytidine induces reversible genome-wide DNA damage that
631 is distinctly influenced by DNA methyltransferases 1 and 3B. Mol Cell Biol *28*, 752-771.
632 Ren, W., Gao, L., and Song, J. (2018). Structural Basis of DNMT1 and DNMT3A-Mediated DNA
633 Methylation. Genes (Basel) *9*.
634 Rowe, L.A., Degtyareva, N., and Doetsch, P.W. (2008). DNA damage-induced reactive oxygen
635 species (ROS) stress response in Saccharomyces cerevisiae. Free Radic Biol Med *45*, 1167-
636 1177.

637 Scott, A., Song, J., Ewing, R., and Wang, Z. (2014). Regulation of protein stability of DNA
638 methyltransferase 1 by post-translational modifications. Acta Biochim Biophys Sin (Shanghai) *46*,
639 199-203.
640 Seo, H.G., Kim, H.B., Kang, M.J., Ryum, J.H., Yi, E.C., and Cho, J.W. (2016). Identification of the
641 nuclear localisation signal of O-GlcNAc transferase and its nuclear import regulation. Sci Rep *6*,
642 34614.
643 Shi, F.T., Kim, H., Lu, W., He, Q., Liu, D., Goodell, M.A., Wan, M., and Songyang, Z. (2013). Ten-
644 eleven translocation 1 (Tet1) is regulated by O-linked N-acetylglucosamine transferase (Ogt) for
645 target gene repression in mouse embryonic stem cells. The Journal of biological chemistry *288*,
646 20776-20784.
647 Shin, H., Cha, H.J., Lee, M.J., Na, K., Park, D., Kim, C.Y., Han, D.H., Kim, H., and Paik, Y.K.
648 (2020). Identification of ALDH6A1 as a Potential Molecular Signature in Hepatocellular Carcinoma
649 via Quantitative Profiling of the Mitochondrial Proteome. J Proteome Res *19*, 1684-1695.
650 Shin, H., Cha, H.J., Na, K., Lee, M.J., Cho, J.Y., Kim, C.Y., Kim, E.K., Kang, C.M., Kim, H., and
651 Paik, Y.K. (2018). O-GlcNAcylation of the Tumor Suppressor FOXO3 Triggers Aberrant Cancer
652 Cell Growth. Cancer Res *78*, 1214-1224.
653 Slawson, C., Copeland, R.J., and Hart, G.W. (2010). O-GlcNAc signaling: a metabolic link
654 between diabetes and cancer? Trends in biochemical sciences *35*, 547-555.
655 Tang, X., Miao, Y., Luo, Y., Sriram, K., Qi, Z., Lin, F.M., Gu, Y., Lai, C.H., Hsu, C.Y., Peterson,
656 K.L., et al. (2020). Suppression of Endothelial AGO1 Promotes Adipose Tissue Browning and
657 Improves Metabolic Dysfunction. Circulation *142*, 365-379.
658 Thurman, R.E., Day, N., Noble, W.S., and Stamatoyannopoulos, J.A. (2007). Identification of
659 higher-order functional domains in the human ENCODE regions. Genome Res *17*, 917-927.
660 Torres, C.R., and Hart, G.W. (1984). Topography and polypeptide distribution of terminal N-
661 acetylglucosamine residues on the surfaces of intact lymphocytes. Evidence for O-linked GlcNAc.
662 The Journal of biological chemistry *259*, 3308-3317.
663 Vasconcelos-Dos-Santos, A., de Queiroz, R.M., da Costa Rodrigues, B., Todeschini, A.R., and
664 Dias, W.B. (2018). Hyperglycemia and aberrant O-GlcNAcylation: contributions to tumor
665 progression. J Bioenerg Biomembr *50*, 175-187.
666 Walgren, J.L., Vincent, T.S., Schey, K.L., and Buse, M.G. (2003). High glucose and insulin
667 promote O-GlcNAc modification of proteins, including alpha-tubulin. Am J Physiol Endocrinol
668 Metab *284*, E424-434.
669 Wang, Y., Chen, L., Pandak, W.M., Heuman, D., Hylemon, P.B., and Ren, S. (2020). High
670 Glucose Induces Lipid Accumulation via 25-Hydroxycholesterol DNA-CpG Methylation. iScience
671 *23*, 101102.
672 Yang, X., and Qian, K. (2017). Protein O-GlcNAcylation: emerging mechanisms and functions.
673 Nature reviews. Molecular cell biology *18*, 452-465.
674 Yang, Y., Fu, M., Li, M.D., Zhang, K., Zhang, B., Wang, S., Liu, Y., Ni, W., Ong, Q., Mi, J., et al.
675 (2020). O-GlcNAc transferase inhibits visceral fat lipolysis and promotes diet-induced obesity. Nat
676 Commun *11*, 181.
677 Yarychkivska, O., Shahabuddin, Z., Comfort, N., Boulard, M., and Bestor, T.H. (2018). BAH
678 domains and a histone-like motif in DNA methyltransferase 1 (DNMT1) regulate de novo and
679 maintenance methylation in vivo. The Journal of biological chemistry *293*, 19466-19475.
680 Yompakdee, C., Bun-ya, M., Shikata, K., Ogawa, N., Harashima, S., and Oshima, Y. (1996). A
681 putative new membrane protein, Pho86p, in the inorganic phosphate uptake system of
682 Saccharomyces cerevisiae. Gene *171*, 41-47.
683 Zhang, Q., Liu, X., Gao, W., Li, P., Hou, J., Li, J., and Wong, J. (2014). Differential regulation of
684 the ten-eleven translocation (TET) family of dioxygenases by O-linked beta-N-acetylglucosamine
685 transferase (OGT). The Journal of biological chemistry *289*, 5986-5996.

686 Zhou, H., Di Palma, S., Preisinger, C., Peng, M., Polat, A.N., Heck, A.J., and Mohammed, S.
687 (2013). Toward a comprehensive characterization of a human cancer cell phosphoproteome.
688 Journal of proteome research *12*, 260-271.
689 Zhou, W., Dinh, H.Q., Ramjan, Z., Weisenberger, D.J., Nicolet, C.M., Shen, H., Laird, P.W., and
690 Berman, B.P. (2018). DNA methylation loss in late-replicating domains is linked to mitotic cell
691 division. Nat Genet *50*, 591-602.
692 Zhou, W., Liang, G., Molloy, P.L., and Jones, P.A. (2020). DNA methylation enables transposable
693 element-driven genome expansion. Proc Natl Acad Sci U S A *117*, 19359-19366.

694 **Figures**

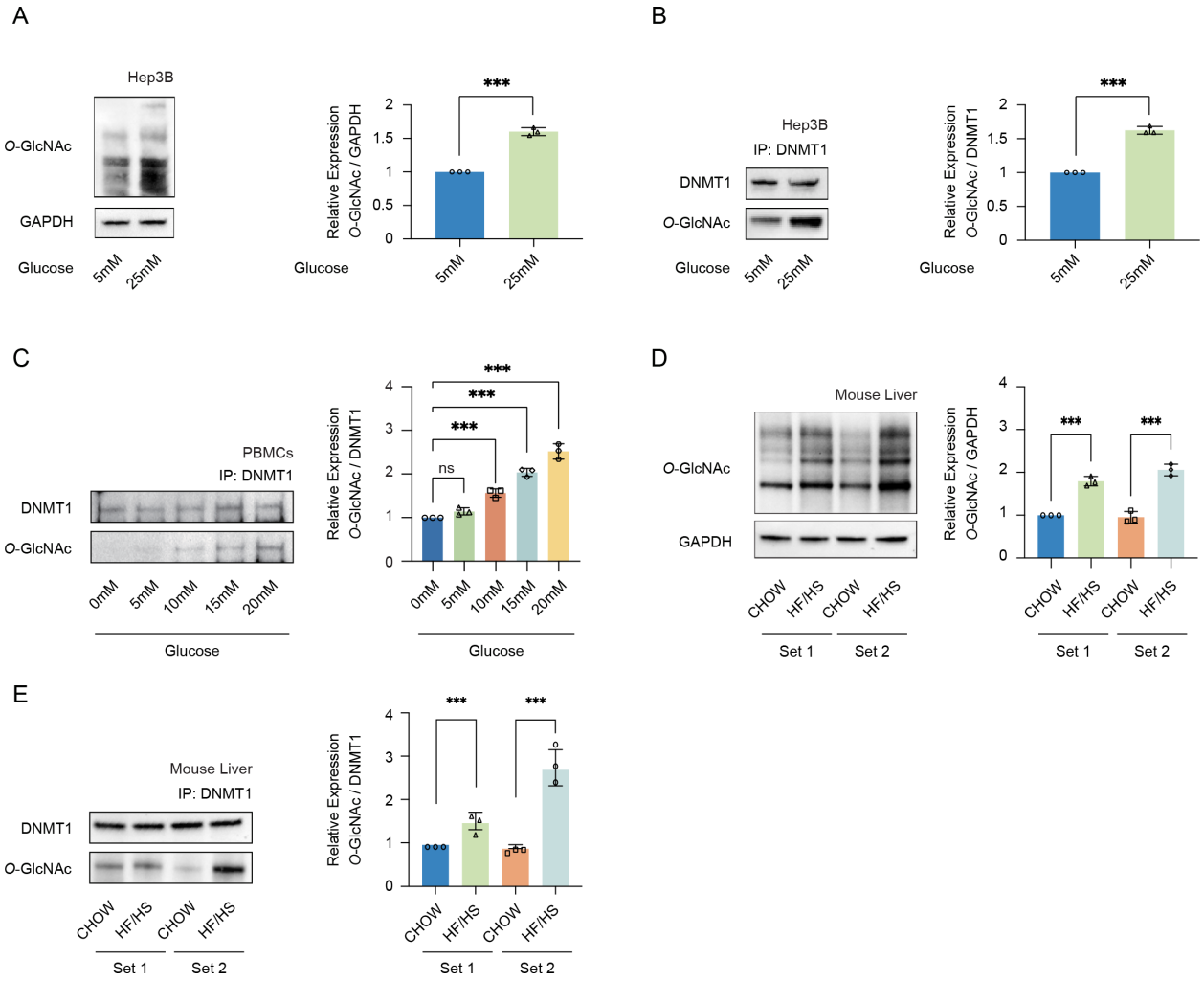

695

696 **Figure 1.** High glucose increases *O*-GlcNAcylation of DNMT1 in cell lines and primary cells. (**A**)
697 Hep3B cells were treated glucose (5mM or 25mM). Shown are immunoblots of collected lysates
698 using antibody targeting *O*-GlcNAc, and GAPDH (n = 3). (**B**) Lysates of Hep3B treated with
699 glucose were immunoprecipitated with DNMT1 and immunoprecipitates were immunoblotted with
700 antibody targeting *O*-GlcNAc (n = 3). (**C**) PBMCs were isolated from three individual donor blood
701 samples and treated with increasing concentration of glucose for 24 hours. Collected cell lysates
702 from PBMCs were immunoprecipitated with antibody targeting DNMT1 and immunoblotted for *O*-
703 GlcNAc. Representative blot from one donor. (n = 3). (**D**) Immunoblots for *O*-GlcNAc, and GAPDH
704 from liver samples of C57BL/6J mice given a high-fat / high-sucrose diet (HF/HS) or normal diet

705 (CHOW) for 4 months. (**E**) Lysates of mouse liver were immunoprecipitated with DNMT1 and
706 immunoprecipitates were immunoblotted with antibody targeting *O*-GlcNAc. ***$p < 0.0001$ by
707 Student's *t*-test (**A**-**E**); ns, not significant; Data are represented as mean ± SD from three
708 replicates of each sample.

709 **Figure supplement 1.** DNMT1 can be *O*-GlcNAcylated in Hep3B cells.

710 **Figure supplement 2.** DNMT1 can be *O*-GlcNAcylated in HepG2 cells and B cells derived
711 lymphocytes.

712 **Figure supplement 3.** Global protein *O*-GlcNAcylation was induced with high concentrations of
713 sucrose.

714 **Figure supplement 4.** The enzymatic activity of OGT or OGA was not significantly changed by
715 glucose treatment.

716 **Figure supplement 5.** DNMT1 can be *O*-GlcNAcylated in primary cells (peripheral blood
717 mononuclear cells, PBMCs).

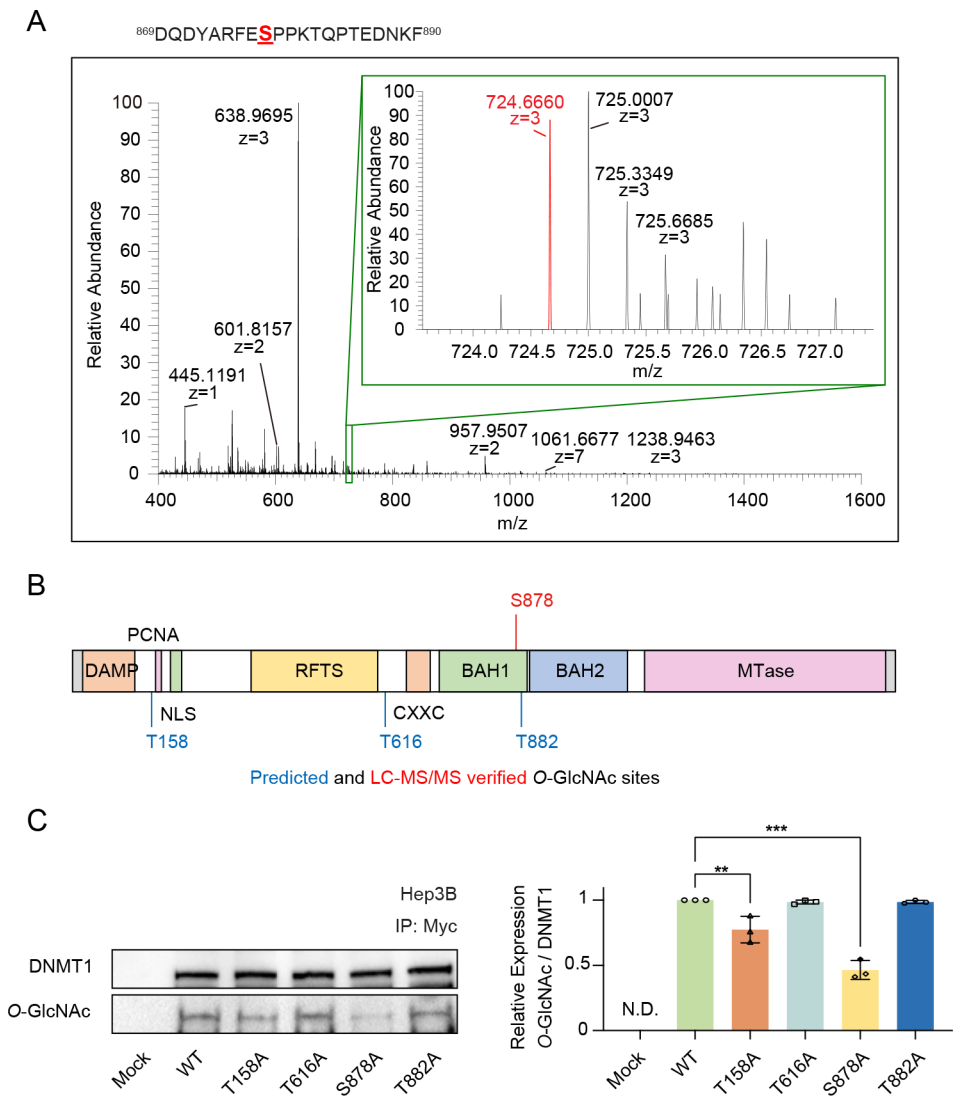

Figure 2. Identification of *O*-GlcNAcylated sites within DNMT1 by LC-MS/MS. (**A**) Schematic drawing of the DNMT1 *O*-GlcNAc modified region enriched from Hep3B cells based on mass spectrometry (MS) data and tandem MS (MS/MS) peaks. FTMS + p NSI Full MS [400.0000-1600.0000]. DQDYARFESPPKTQPTEDNKF (S9 HexNAc) – S878. (**B**) Schematic diagram of identified novel *O*-GlcNAcylated sites within DNMT1 as determined via LC-MS/MS and OGTSite. DMAP, DNA methyltransferase associated protein-binding domain; PCNA, proliferating cell nuclear antigen-binding domain; NLS, nuclear localization sequences; RFTS, replication foci targeting sequence domain; BAH, bromo-adjacent homology domain. (**C**) Each immunoprecipitated Myc-DNMT1 wild type and substituted mutants was immunoblotted with an

728 *O*-GlcNAc antibody ($n = 3$). **$p < 0.0005$; ***$p < 0.0001$ by Student's *t*-test (**C**); N.D., not detected;

729 Data are represented as mean ± SD from three replicates of each sample.

730 **Figure supplement 1.** Myc-DNMT1-WT in Hep3B cells can be *O*-GlcNAcylated.

731 **Figure supplement 2.** Tandem MS/MS peaks of *O*-GlcNAcylated DNMT1 peptides.

732 **Figure supplement 3.** Loss of both threonine and serine in DNMT1 (DNMT1-T158A/S878A)

733 resulted in a loss of *O*-GlcNAcylation.

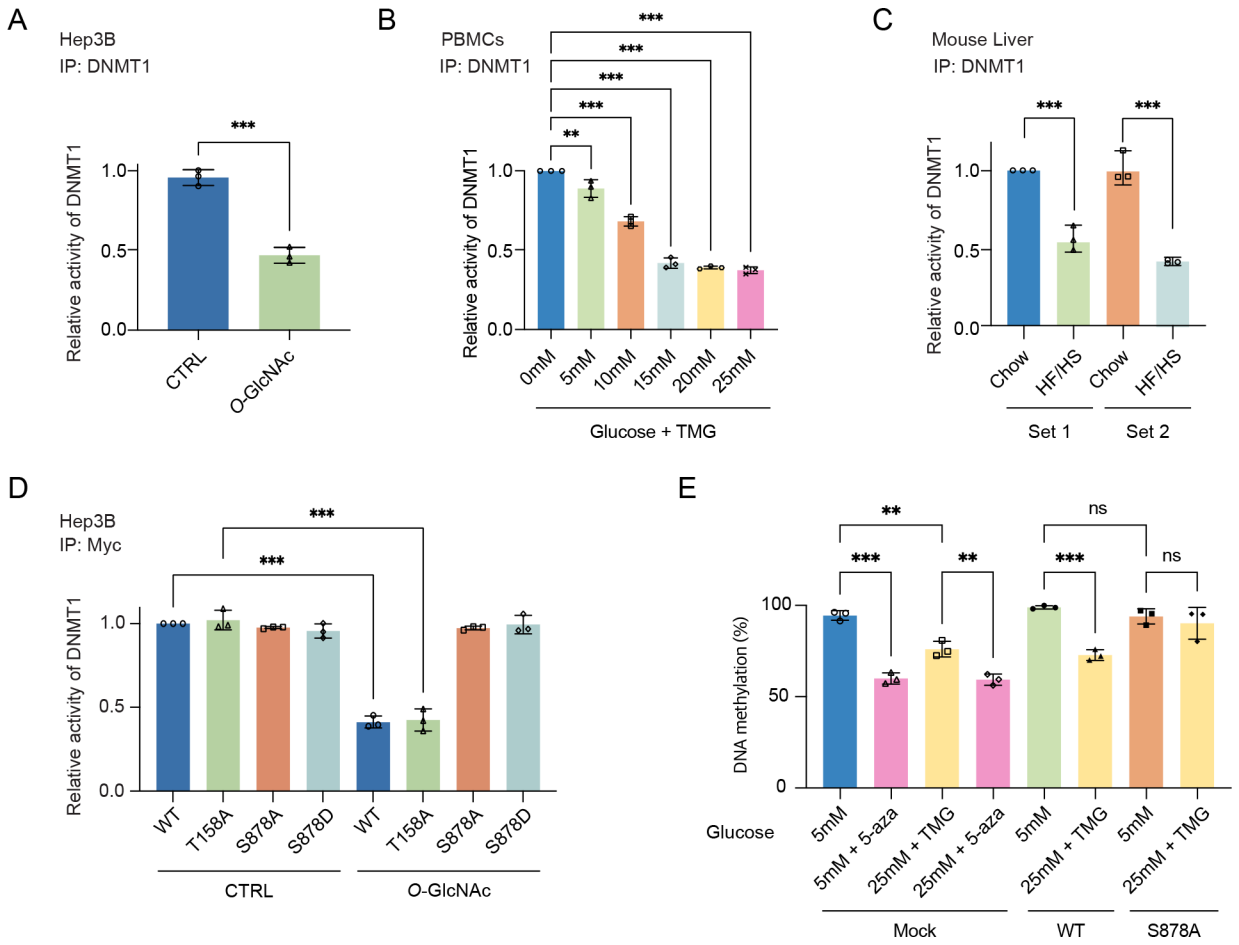

Figure 3. Site specific *O*-GlcNAcylation inhibits DNMT1 methyltransferase function. For (**A-D**), bar graphs are of relative activity of DNA methyltransferase activity measured as absorbance from a DNMT Activity/Inhibition ELISA kit and representative immunoblots of immunoprecipitates performed with antibodies targeting DNMT1. (**A**) Hep3B cells were treated with 5mM (CTRL) or 25mM glucose with TMG (*O*-GlcNAc) (n = 3). (**B**) PBMCs from donors were treated with increasing concentrations of glucose (range: 0-25mM with TMG) (n = 3). (**C**) Liver samples from C57BL/6J mice given a HF/HS diet or a normal diet (CHOW) for 4 months. (**D**) Immunoprecipitated DNMT1 wild type and substituted mutants were treated with 5mM or 25mM glucose (n = 3). (**E**) Each Hep3B and Myc-DNMT1 overexpressed mutant (DNMT1-WT or DNMT1-S878A) was treated with 5mM or 25mM glucose or 5-aza (negative control). Shown are absorbance of global DNA methylation of LINE-1 performed with global DNA methylation LINE-1

746 kit. (n = 3). **p < 0.005; ***p < 0.0001 by Student's t-test (**A**-**E**); ns, not significant; Data are
747 represented as mean ± SD from three replicates of each sample.
748 **Figure supplement 1.** Site specific *O*-GlcNAcylation at DNMT1 sites abrogate the function of
749 methyltransferase and DNA loss of methylation at CpG island under high glucose/TMG conditions.
750 **Figure supplement 2.** The methylation loss by high glucose/TMG conditions was not apparent
751 in the DNMT1-S878A mutant.

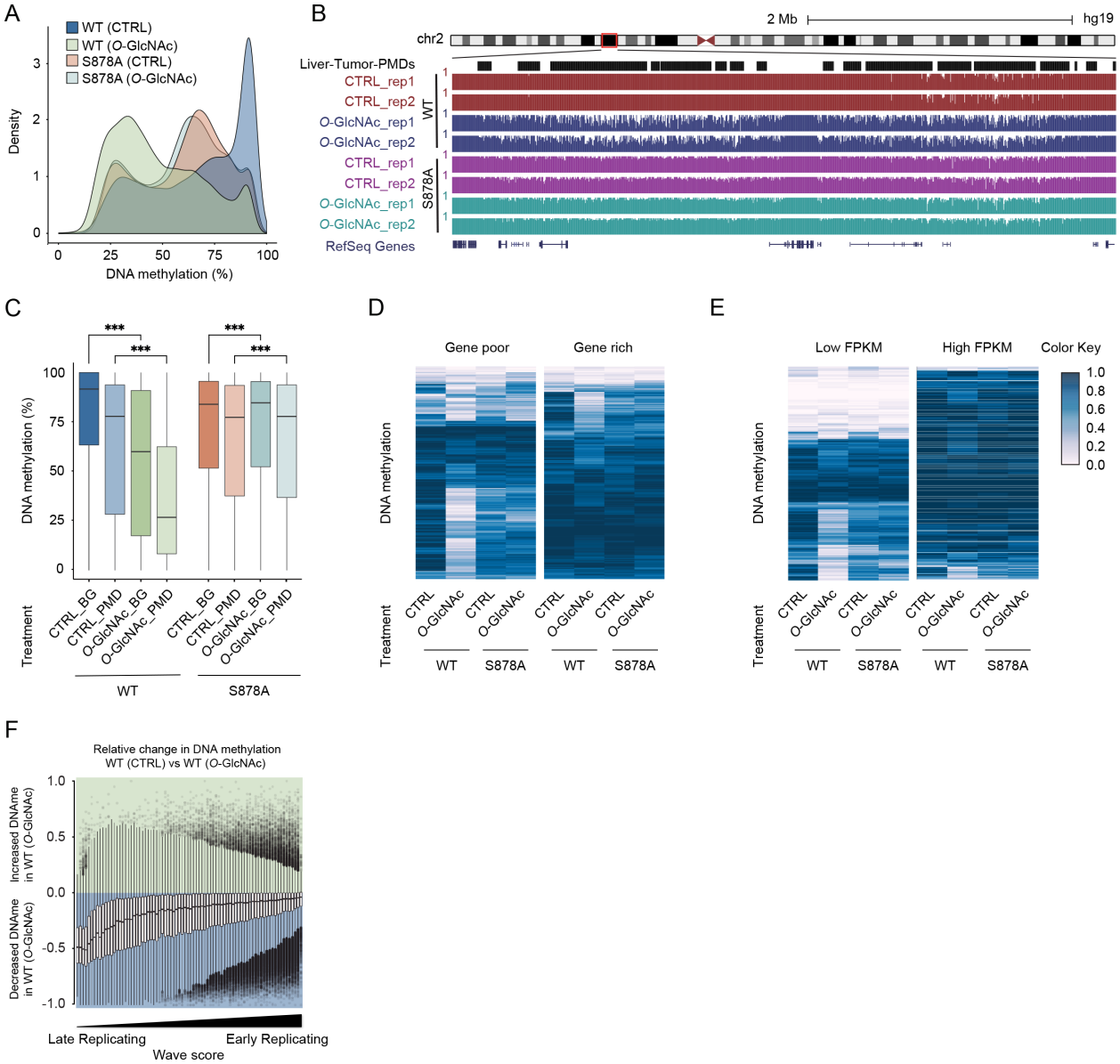

Figure 4. High glucose leads to loss of DNA methylation at cancer specific partially methylated domains (PMDs). (**A**) Density plot of DNA methylation for DNMT1-WT and DNMT1-S878A cells and low (5mM, CTRL) or high glucose with TMG (25mM, *O*-GlcNAc). (**B**) Genome browser screenshot of DNA methylation for DNMT1-WT and DNMT1-S878A cells and low or high glucose along with liver tumor PMDs from (Li et al., 2016). (**C**) Boxplots of DNA methylation at PMDs or general genomic background (BG) for each DNMT1-WT and DNMT1-S878A treated with low (5mM, CTRL) or high glucose with TMG (25mM, *O*-GlcNAc). (**D**) Heatmap representation of global DNA methylation for DNMT1-WT and DNMT1-S878A cells under low (5mM, CTRL) or high

761 glucose with TMG (25mM, *O*-GlcNAc) at gene poor and gene rich regions. (**E**) Heatmap represent
762 global DNA methylation of wild type and DNMT1 mutants between low FPKM regions and high
763 FPKM regions (DNMT1-WT or DNMT1-S878A) which treated low (5mM, CTRL) or high glucose
764 with TMG (25mM, *O*-GlcNAc) were determined by Nanopolish call methylation. These are defined
765 'low FPKM' as containing less than 25% of RPKM regions per Mb window, and 'high FPKM' as
766 containing more than 75% of RPKM regions per Mb window. (**F**) Methylation changes from *O*-
767 GlcNAcylation of DNMT1 by wave score for replication timing (Hansen et al., 2010; Thurman et
768 al., 2007). ***$p < 0.0001$ by Wilcoxon signed-rank test (**C**).

769 **Figure supplement 1.** DNA loss of methylation by increased global *O*-GlcNAcylation decreases.
770 Density plot of DNA methylation for DNMT1-WT and DNMT1-S878A cells and low or high glucose.

771 **Figure supplement 2.** Methylation changes from *O*-GlcNAcylation of DNMT1 in DNMT1-S878A
772 mutant. The loss of methylation was not observed in DNMT1-S878A mutant cells.

773 **Figure supplement 3.** DNA loss of methylation by increased global *O*-GlcNAcylation decreases
774 around the transposable elements (TEs) regions.

775 **Figure supplement 4.** Evolutionarily recent TEs are more likely to lose methylation than older
776 elements in a variety of systems.

777 **Figure supplement 5.** ZFP57 and ZNF605 demonstrate binding to a significant number of
778 LTR12C elements present in liver cancer PMDs.

779 **Figure supplement 6.** Evolutionarily recent elements are less likely to lose methylation induced
780 by *O*-GlcNAcylation of DNMT1.

781 **Figure supplement 7.** Only loci with greater than 5x coverage were retained for analysis,
782 comprising 90% of CpGs in the genome.

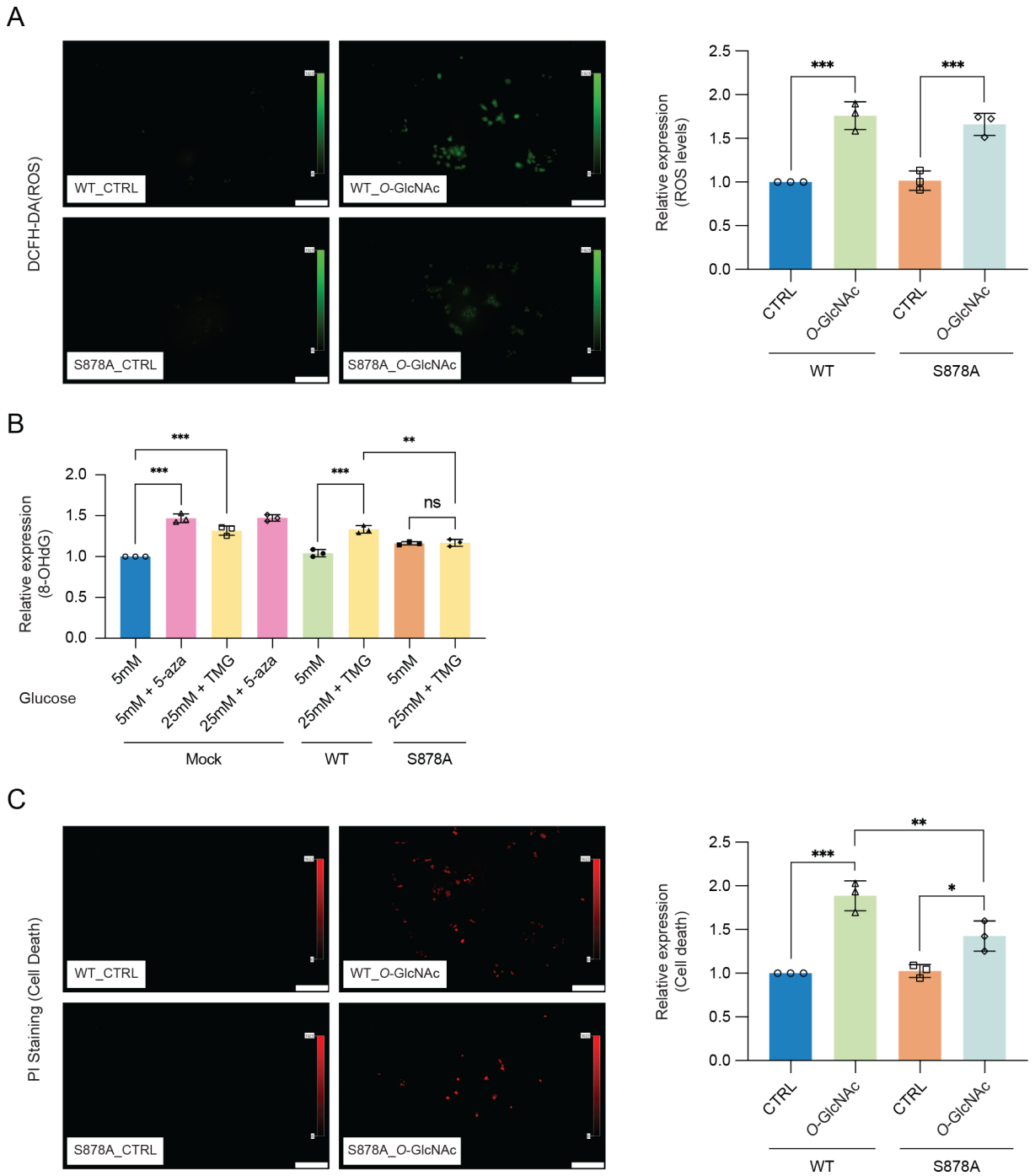

Figure 5. High glucose induced reactive oxygen species (ROS) and DNA damage cause apoptotic cell death in DNMT1-WT cells. (**A**) Quantitative fluorescence image of reactive oxygen species (ROS) in DNMT1-WT and DNMT1-S878A cells and low (5mM, CTRL) or high glucose with TMG (25mM, *O*-GlcNAc). (**B**) Each Hep3B and Myc-DNMT1 overexpressed mutant (DNMT1-WT or DNMT1-S878A) was treated with 5mM or 25mM glucose or 5-aza (negative control).

789 Shown are absorbance of 8-OHdG performed with DNA damage quantification kit. (n = 3). (**C**)
790 Quantitative fluorescence image of cell death in propidium iodide staining of DNMT1-WT and
791 DNMT1-S878A cells and low (5mM, CTRL) or high glucose with TMG (25mM, *O*-GlcNAc). *p <
792 0.001; **p < 0.005; ***p < 0.0001 by Student's *t*-test (**A**-**C**); ns, not significant; Data are
793 represented as mean ± SD from three replicates of each sample.
794 **Figure supplement 1.** Heatmap representation of promoter DNA methylation for DNMT1-WT
795 and DNMT1-S878A cells under with low (5mM, CTRL) or high glucose with TMG (25mM, *O*-
796 GlcNAc) at gene poor and gene rich regions.
797 **Figure supplement 2.** DNA loss of methylation within promoter region by increased global *O*-
798 GlcNAcylation impact different gene pathways.
799 **Figure supplement 3.** Quantitative analysis of human apoptosis related proteins in DNMT1-WT
800 and DNMT1-S878A by high glucose treatment using Proteome profiler.